IOPscience iopscience.iop.org

Home Search Collections Journals About Contact us My IOPscience

Polarization-dependent femtosecond laser ablation of poly-methyl methacrylate

This article has been downloaded from IOPscience. Please scroll down to see the full text article.

2012 New J. Phys. 14 085010

(http://iopscience.iop.org/1367-2630/14/8/085010)

View the table of contents for this issue, or go to the journal homepage for more

Download details:
IP Address: 137.122.30.96
The article was downloaded on 18/03/2013 at 20:47

Please note that terms and conditions apply.

New Journal of Physics
The open-access journal for physics

Polarization-dependent femtosecond laser ablation of poly-methyl methacrylate

J-M Guay, A Villafranca, F Baset, K Popov, L Ramunno and V R Bhardwaj[1]

Department of Physics and Center for Research in Photonics, University of Ottawa, 150 Louis Pasteur, Ottawa, ON, K1N 6N5, Canada
E-mail: ravi.bhardwaj@uottawa.ca

New Journal of Physics **14** (2012) 085010 (17pp)
Received 17 February 2012
Published 17 August 2012
Online at http://www.njp.org/
doi:10.1088/1367-2630/14/8/085010

Abstract. We show that ablation features in poly-methyl methacrylate (PMMA) induced by a single femtosecond laser pulse are imposed by light polarization. The ablation craters are elongated along the major axis of the polarization vector and become increasingly prominent as the pulse energy is increased above the threshold energy. We demonstrate ~40% elongation for linearly and elliptically polarized light in the fluence range of 4–20 J cm^{-2}, while circularly polarized light produced near circular ablation craters irrespective of pulse energies. We also show that irradiation with multiple pulses erases the polarization-dependent elongation of the ablation craters. However, for line ablation the orientation of the electric field vector is imprinted in the form of quasi-periodic structures inside the ablated region. Theoretically, we show that the polarization dependence of the ablation features arises from a local field enhancement during light–plasma interaction. Simulations also show that in materials with high nonlinearities such as doped PMMA, in addition to conventional explosive boiling, sub-surface multiple filamentation can also give rise to porosity.

[1] Author to whom any correspondence should be addressed.

© IOP Publishing Ltd and Deutsche Physikalische Gesellschaft

Contents

1. Introduction

Light–matter interactions are often governed by the intensity, wavelength and polarization of light. When ultrafast lasers are used, pulse duration also affects the energy coupling and dissipation in the system. The role of polarization of light in the interaction of atoms and molecules with intense femtosecond light pulses is well understood and is often exploited to align molecules [1–3] and to control electron dynamics in the laser field with a high degree of spatial and temporal precision [4, 5]. The latter is crucial in attosecond science [6, 7]. However, the role of polarization in the interaction of intense light pulses with solids is subtle and not clear.

The interaction of tightly focused intense femtosecond light pulses with solids often leads to ablation of the material surface or refractive index modification in transparent materials [8, 9]. Several mechanisms are involved in the interaction, some of which depend on the laser polarization that can potentially leave an imprint on the modification/ablation process. For example, both processes (ablation/modification) are initiated by multi-photon ionization that depends on light polarization. In crystalline dielectrics, multi-photon ionization depends on sample orientation due to direction dependence of the effective mass of the electron [10]. This is similar to multi-photon ionization in molecules where the rates differ by more than 50% depending on the alignment of the molecular axis with respect to linearly polarized light [11, 12].

In addition to multi-photon ionization, impact ionization can also occur, rapidly increasing the carrier density and forming a plasma that either expands (as in ablation) or is confined in the bulk (as in internal modification). Subsequent interaction of the incident light with the plasma can lead to polarization-dependent absorption. Experiments on laser-produced plasmas have demonstrated sharp differences (up to 50–60%) in absorption of p- and s-polarized light due to resonance absorption [13, 14]. In addition, the interaction of linearly polarized light with dense plasma can also lead to local field enhancements akin to that observed in metal nanoparticles [15].

To date, signatures of polarization-dependent phenomena have been observed mostly in the multiple pulse regime both on surfaces and inside bulk materials. Polarization-dependent

self-organized three-dimensional (3D) periodic nanostructures have been observed inside fused silica [16, 17] under irradiation with multiple light pulses. For linearly polarized light, bulk grating-like structures were formed orthogonal to the laser polarization and their origin was attributed to local field enhancement arising from light–plasma interaction [17–19]. Such polarization-dependent nanostructures have found applications in rewritable 3D data storage [20], embedded microarray optics and microfluidics [21, 22]. For circularly polarized light, the handedness of the light was imprinted in the form of ordered sub-micron chiral structures [23]. The ability to imprint the electric field in the form of oriented nanostructures has recently been exploited to develop a sub-wavelength resolution diagnostic tool to visualize the complex polarization state of the light in the focal volume [24].

Laser-induced polarization-dependent periodic structures (or surface ripples) have also been observed on surfaces in the ablation crater of a variety of materials including dielectrics, semiconductors and metals under widely different illumination conditions [25–28]. Ripple spacing of the order of wavelength to sub-wavelength [29–34] has been observed and varies with the fluence and the number of laser pulses. Moreover, the structures have been found to be predominantly perpendicular to the laser polarization. The ripple formation is described in terms of interference between the incident light and the surface scattering wave [35] or surface plasmon polaritons [36]. Ripple structures parallel to the laser polarization have also been observed in the ablation crater [37, 38].

Apart from surface ripples within the interaction region the overall features of the ablation region were found to be polarization dependent. Experiments on multiple pulse ablation of thin metal films exhibited elongation of the ablation craters along the major axis of the polarization vector when the pulse energy was close to the ablation threshold [39]. The elongation of ablation features gradually disappeared when the pulse energy was increased beyond the threshold value by $\sim$50%.

In this paper, we present a complete experimental and numerical study of polarization-dependent ablation of poly-methyl methacrylate (PMMA). In section 2, we describe the experimental setup and present the evolution of ablation features as a function of the pulse energy and the number of laser shots. We show that the ablation craters in PMMA are elongated along the major axis of the polarization vector whenever pulse energies exceeded the threshold value. Only circularly polarized light produces near circular ablation craters irrespective of pulse energies. We also show that the polarization-dependent elongation of the ablation craters vanishes for multiple laser pulses. However, for line ablation the polarization dependence is preserved in the form of quasi-periodic structures which are oriented along the laser polarization.

In section 3, we describe the 3D finite-difference time domain (FDTD) simulation of the interaction of intense light pulses with PMMA and compare it with the experimental results. This approach determines energy deposition patterns and assumes that all of the absorbed energy is eventually transferred to the lattice, resulting in ablation/modification. We show that elongation of ablation craters arises from the local field enhancement during light–plasma interaction. When the initial plasma density is above the critical density (where the light frequency is equal to the plasma frequency), field enhancement occurs parallel to the laser polarization. Faster plasma growth in the regions with enhanced fields results in an asymmetric plasma density profile, which when transferred to the lattice leads to elongation of the ablation crater. We conclude by showing that in doped PMMA with very high third-order susceptibility

sub-surface multiple filamentation can give rise to induced porosity in addition to conventional explosive boiling.

2. Polarization dependence of ablation

2.1. Experimental methods

In our experiments, 800 nm light from a Ti:sapphire laser system, operating at a repetition rate of 5 kHz and producing 45 fs pulses with a peak energy of 0.5 mJ, was focused on the surface of PMMA by a 0.25 NA (10×) microscope objective. The back aperture of the microscope objective (8 mm) was slightly overfilled to minimize alignment errors. The position of the laser focus relative to the surface of optically polished bulk PMMA samples ($12.5 \times 12.5 \times 1.7\,\mathrm{mm}^3$) was accurately determined by imaging the back reflected light with a CCD camera at very low pulse energies below the ablation threshold. After locating the surface of PMMA, the glass plate at 45°, used for directing the back reflected light, was removed in order to avoid distortion of the incident polarization.

A gradient neutral density filter was used to vary the pulse energy from 50 nJ to 5 μJ. The step size of 100 nJ was used to determine the single and multiple shot ablation thresholds. For this the laser was operated either in a single shot or in continuous mode. In the latter, the sample speed was selected such that a specific number of pulses was incident within the focal region. The PMMA sample was mounted on three-axis translation stages with a resolution of 50 nm along the lateral dimensions (X, Y) and 100 nm along the axial direction (Z). The lowest energy at which ablation features were visible under the scanning electron microscope (SEM) was defined as the threshold value. A calibrated fast photodiode operating in the linear regime monitored the incident power. The spot size was obtained from the slope of a semi-logarithmic plot of the squared diameter of the modified region measured with an SEM image as a function of pulse energy [40]. We obtained a Gaussian beam radius of $2.6 \pm 0.2\,\mu$m for the 0.25 NA microscope objective (close to the diffraction-limited beam radius of $\sim 2\,\mu$m) and used it to calculate the laser fluence values.

To study the polarization dependence, the pulse energy was varied from the threshold value in steps of 0.5 μJ. A quarter waveplate was used to produce elliptical or circular polarizations. To select s or p polarizations a polarizer was placed after the quarter waveplate. Switching the relative position of the two optics ensured that the pulse duration remained the same while changing the polarization. A thin broadband beam sampler at the output of the laser directed a small fraction of the beam into a single-shot autocorrelator to monitor the pulse duration continuously. The pulse duration at the back aperture of the objective was measured to be 70 fs after propagating through all the optics. The pulses were not pre-chirped. The incident pulse energies were measured after the microscope objective taking into account the transmission and reflection losses of all the optics.

2.2. Single-shot ablation of poly-methyl methacrylate (PMMA)

Figure 1 shows the polarization dependence of single-shot laser ablation of PMMA obtained with a pulse energy of 3.2 μJ that is ~5 times higher than the threshold value. The SEM images reveal two interesting aspects of the interaction. Firstly, the ablation craters are elongated along the major axis of the polarization vector for both linear (figures 1(a) and (b)) and elliptically

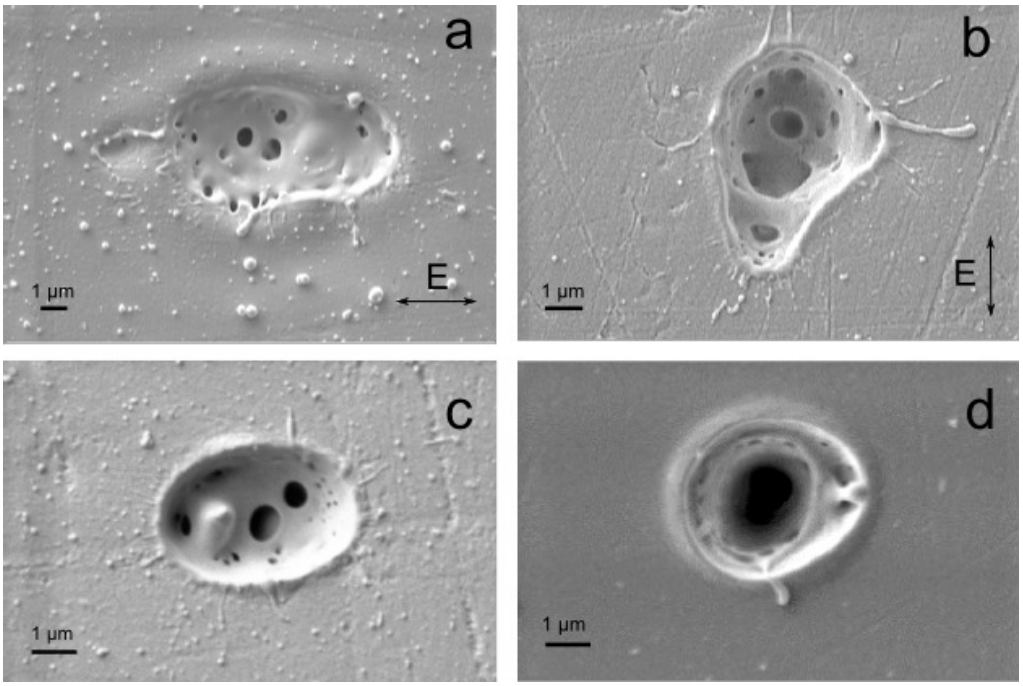

Figure 1. SEM images of single-shot ablation craters in PMMA produced by different polarizations of incident light: (a) p polarization, (b) s polarization, (c) elliptical polarization (ϵ = 0.5) and (d) circular polarization (ϵ = 0.9). $\epsilon = E_y/E_x$ is the ellipticity of light defined as the ratio of the electric fields in the two orthogonal directions. The pulse energy was 3.2 μJ, measured after the microscope objective corresponding to a laser fluence of 14.3 J cm^{-2}.

(figure 1(c)) polarized light. The ellipticity $\epsilon = E_y/E_x$, defined as the ratio of the electric fields along the two orthogonal axes, is 0.5 for the latter. Only circularly polarized light was produced near circular ablation craters (figure 1(d)), suggesting that the mechanism responsible for elongation can be turned on or off by laser polarization. The small asymmetry that can be seen in figure 1(d) is due to the fact that polarization is not perfectly circular ($\epsilon = 0.9$ instead of 1).

Secondly, the ablation of PMMA is not homogeneous; instead nanostructures are formed within the interaction region. Associated with this is the observation of nanodroplets in adjacent regions, suggesting localized melting and nano-explosions that render the material porous (see also figure 4). This process, called explosive boiling, is specific to ultrashort pulse laser irradiation where near isochoric heating and rapid adiabatic expansion result in material ejection [41–46]. While most experiments to date have studied this effect by post-mortem analysis of the laser-induced damage, only a few time-resolved experiments have investigated the fundamental physical mechanisms of the ablation process [47]. There is general consensus that after thermalization of the laser energy in the material (on the ps time scale) a two-phase liquid–gas mixture develops, which then undergoes hydrodynamic expansion, resulting in material ejection and subsequent resolidification on the ns time scale [48, 49]. It is interesting to note that both elongation of the ablation crater and formation of nanostructures within do not occur at energies close to the ablation threshold.

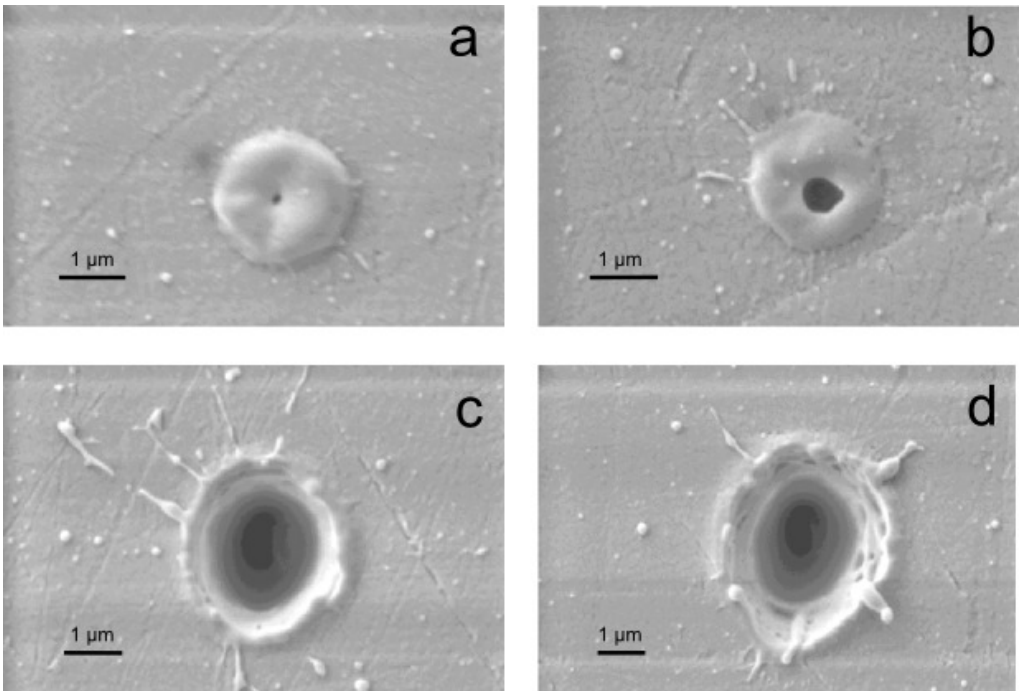

Figure 2. SEM images of single-shot ablation craters produced by s-polarized light with different pulse energies incident on PMMA. (a) 640 nJ, (b) 690 nJ, (c) 1 μJ and (d) 2.1 μJ correspond to laser fluences of 2.9, 3.1, 4.5 and 9.4 J cm^{-2}, respectively.

Figure 2 shows the evolution of single-shot ablation of PMMA as a function of pulse energies. At threshold energies, ablation occurs in a circular region starting with a swelling of the material followed by material ejection (figures 2(a) and (b)). This eliminates beam distortions as a potential contributor to elongation of ablation craters. When the pulse energy is increased, the ablation crater starts elongating along the polarization direction (figures 2(c) and (d)). Also, nanostructures start appearing along the edges (figure 2(d)) and grow into the middle as well (figure 1(a)). Figures 2(a) and (b) are reminiscent of pronounced surface swelling due to a two-phase expanding mixture that fills the volume between the shell and the bottom of the crater, followed by material expulsion [50, 51].

The polarization dependence of ablation as a function of fluence can be summarized for different polarizations in terms of an asymmetry parameter defined as the ratio of the crater dimensions along the two orthogonal axes as shown in figure 3. Near the threshold fluences, all three polarizations produce nearly identical circular ablation features (the asymmetry value is unity). At approximately twice the threshold fluence, linear and elliptical polarizations produce asymmetric ablation craters, while the circular polarization still gives rise to an asymmetry of unity. This trend continues as the fluence increases by a factor of five. Linear and elliptical polarizations introduce an up to 40% change in the asymmetry value. The 5% change in the asymmetry associated with circular polarization could be due the value of ϵ being 0.9 instead of 1.

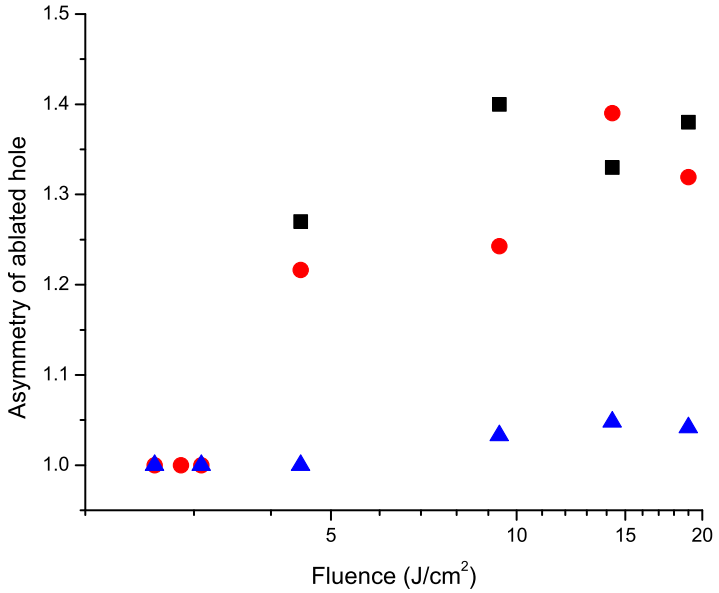

Figure 3. Asymmetry of the ablation crater as a function of laser fluence for different polarizations: linear polarization (●), elliptical polarization (■) and circular polarization (▲). The asymmetry of the ablation crater is the ratio of the dimensions along two orthogonal directions. The size of the symbols represents the errors bars.

2.3. Shot-to-shot evolution of ablation

The shot-to-shot evolution of the ablation of PMMA is shown in figure 4. Firstly, the asymmetry of the ablation crater observed with a single laser pulse disappears when multiple laser pulses are used. This effect is contrary to the observation of periodic structures inside fused silica [16, 17] and the elongation of ablation features on thin metal films [39] where multiple pulses were essential for their formation. A combination of induced porosity and modification of the material by successive laser pulses that alter the coupling of light into PMMA leads to disappearance of the polarization-dependent elongation. Secondly, the porosity evolves from being a 2D to a 3D effect as the hole gets deeper, leading to a quasi-honeycomb-like structure on the side walls (figure 4(c)).

To investigate multi-shot effects on ablation, we studied the threshold fluence as a function of the number of laser shots as shown in figure 4(d). The number of laser shots is selected by triggering the laser externally (red circles) or by moving the laser focus at speeds such that the chosen number of laser pulses were incident within the focal region (black squares). The single-shot ablation threshold of $2.6\,\mathrm{J\,cm^{-2}}$ for PMMA is in good agreement with the published data [40, 52]. However, we observe that the two- and three-shot ablation thresholds decrease faster than the reported values. As the number of laser shots increases further, the threshold fluence decreases rapidly and then saturates. This behaviour corresponds to shot-to-shot memory in the ionization of PMMA, the first step in the ablation process. This is also called the incubation effect [40]. In fused silica, memory has been associated with the change in band gap of the material where successive laser shots alter the material properties, making it easier to ionize [53].

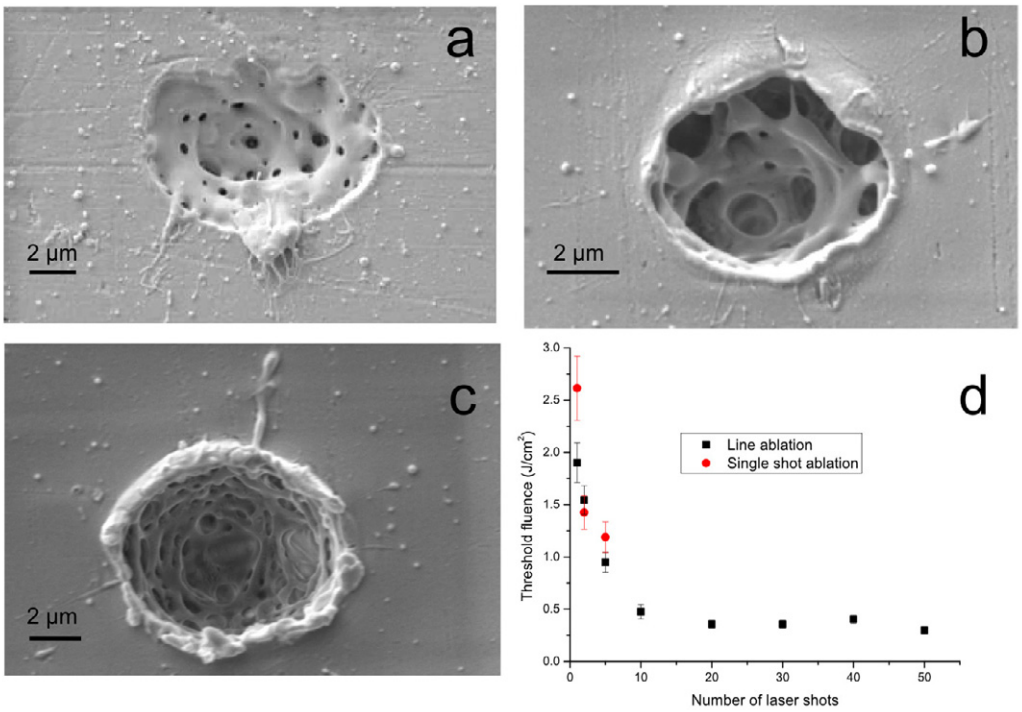

Figure 4. Shot-to-shot evolution of ablation in PMMA. SEM images of ablated regions with (a) one, (b) two and (c) five laser pulses of energy 4 μJ corresponding to a laser fluence of 19 J cm^{-2}. (d) The ablation threshold as a function of the number of laser shots. Solid circles (solid squares) are obtained by operating the laser in a single-shot mode (continuous shot mode). In the continuous shot mode, the sample speed determined the number of laser shots incident within the focal region.

2.4. Line ablation

When the laser focus is stationary, polarization-dependent elongation of the ablation crater disappears with multiple laser pulses (figures 4(a)–(c)). However, signatures of polarization dependence of the ablation features persist even when the laser focus is moved continuously at different speeds such that the number of pulses incident within the focal area varies. Figure 5 shows the SEM images of ablation lines for different orientations of linearly polarized light. The pulse energy and sample speed were 0.5 μJ and 0.5 mm s^{-1} ($\sim$10 pulses μm^{-1}), respectively. Firstly, the width of the ablation line varies with the angle, θ, between the polarization direction and the direction of motion of the sample. It is maximum when $\theta = 90^{\circ}$(2.2 μm) and decreases to 2.0 μm for $\theta = 45^{\circ}$ and is minimum at $\theta = 0^{\circ}$(1.85 μm). This is consistent with the previous observation of the Kerf width on thin metal films [39].

Secondly, quasi-periodic structures are formed inside the ablated region whose orientation is parallel to the laser polarization. In contrast, internal modification of fused silica resulted in periodic structures which formed perpendicular to the laser polarization [17]. In both the cases the structure is preserved even when the laser focus is moved continuously. As we will show below, the elongation of ablated regions and the orientation of the sub-structures inside arise from local field enhancements during light–plasma interaction. Differences in the orientation

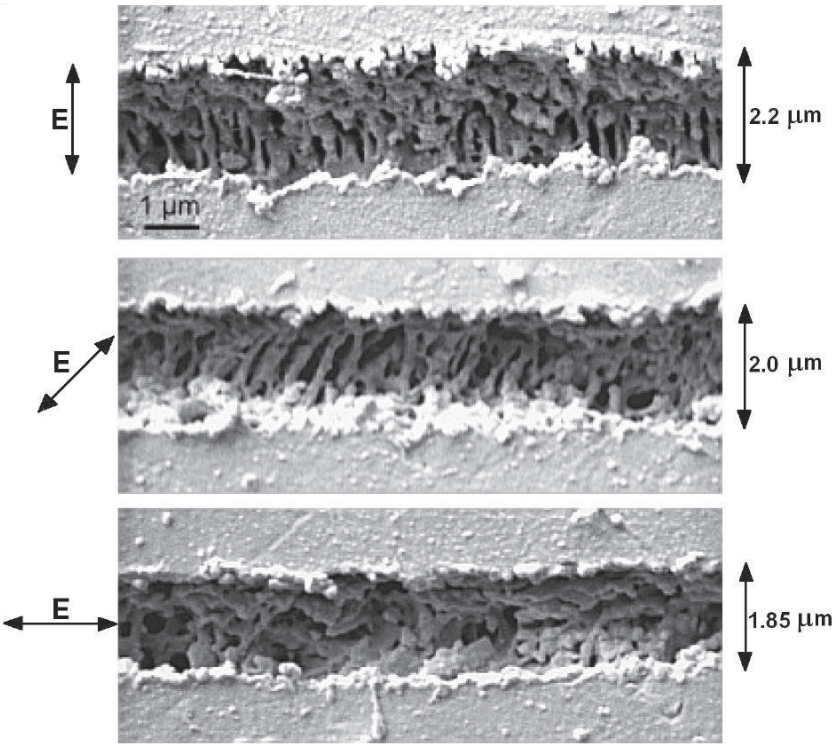

Figure 5. SEM images of ablated lines in PMMA. Arrows on the left indicate the orientation of the laser polarization with respect to the direction of motion of the sample. The width of the ablation lines is shown on the right. The pulse energy was 0.5 μJ and the sample speed was 0.5 mm s^{-1}.

of the quasi-periodic structures during ablation (internal modification) are associated with an overcritical (undercritical) plasma density.

3. Numerical simulation of PMMA ablation

3.1. Theoretical methods

During the laser interaction with materials, the laser energy is initially coupled to the electrons. On a time scale longer than the incident pulse duration, electron–electron and electron–ion collisions lead to thermalization, establishing a Fermi distribution within the excited electron population in the conduction band. On a much longer time scale, electrons transfer their energy to the lattice through electron–phonon coupling. Theoretically, it is challenging to develop a self-consistent hybrid model that considers both the dynamics of free electrons induced by multi-photon, tunnelling and electron impact ionizations as well as electron–electron thermalization and electron–phonon coupling that ultimately transfers energy from the electronic subsystem to the lattice.

To overcome this difficulty, two different approaches are widely employed for studying laser ablation. In the first approach, the initial energy deposition patterns are assumed, and the internal distribution of the deposited energy is followed to study ablation dynamics. Hydrodynamic and molecular dynamic models that take into account atom kinetics belong

to this category. In the second approach, energy deposition patterns are determined, and it is assumed that all the absorbed energy is finally transferred to the lattice, resulting in ablation/modification that takes the shape of the plasma. It is a good approximation due to the large difference in heat capacity of the free-electron gas and phonons. Modelling the dynamics of free electrons in the conduction band by solving electrodynamic, nonlinear Schrodinger and multiple rate equations falls into this category. We use this approach to study polarization-dependent ablation of PMMA.

We have performed FDTD simulations of the fs-scale interaction process between the intense laser pulse and the PMMA sample. A detailed description of our simulation tools is given in [19]. In short, our FDTD code solves the 3D Maxwell equations in a non-magnetic material,

$$\nabla \times \vec{E} = -\frac{1}{c}\frac{\partial \vec{B}}{\partial t}, \quad \nabla \times \vec{B} = \frac{1}{c}\frac{\partial \vec{D}}{\partial t} + \frac{4\pi}{c}\vec{J}, \tag{1}$$

where $\vec{E}$ is the electric field, $\vec{D}$ the electric displacement field and $\vec{J}$ the current density. The displacement field represents the linear and third-order responses of the unmodified dielectric medium, $\vec{D} = \left[1 + 4\pi(\chi^{(1)} + \chi^{(3)}E^2)\right]\vec{E}$, where $\chi^{(1)}$ and $\chi^{(3)}$ are (frequency-independent) first- and third-order susceptibilities of the medium, respectively. The current density $\vec{J}$ is composed of two components: $\vec{J} = \vec{J}_{\mathrm{P}} + \vec{J}_{\mathrm{MPA}}$, where $\vec{J}_{\mathrm{P}}$ represents the free plasma electron motion and $\vec{J}_{\mathrm{MPA}}$ is the effective current accounting for the laser energy loss due to multi-photon absorption (or ionization process) [19, 54, 55]. The free-electron current density is evaluated in our model from the cold plasma hydrodynamics equations

$$\vec{J}_{\mathrm{P}} = -en\vec{u}, \quad \frac{\partial n}{\partial t} = \frac{\partial n_{\mathrm{MPI}}}{\partial t}, \quad \frac{\partial \vec{u}}{\partial t} = -\frac{e}{m}\vec{E} - \Gamma\vec{u}, \tag{2}$$

where n and $\vec{u}$ are plasma particle density and fluid velocity, respectively, $\partial n_{\mathrm{MPI}}/\partial t$ is the rate of change of density due to multiphoton ionization, e and m the electron charge and mass, respectively, and Γ (a constant) is the damping factor due to collisional laser energy absorption in plasma, estimated below using the Spitzer formula [56]. Equation (2) can also be identified with the equation of motion for free particles in the Drude model [57]. We assume in the simulations that the leading ionization process in PMMA is three-photon absorption, resulting in

$$\frac{\partial n_{\mathrm{MPI}}}{\partial t} = \sigma_3 I^3 \frac{n_{\mathrm{s}} - n}{n_{\mathrm{s}}}, \tag{3}$$

where σ_3 is the three-photon absorption cross-section, $I = \frac{c}{4\pi}\langle E^2\rangle$ is the laser intensity and n_{s} is the saturation density, which is estimated for PMMA as $n_{\mathrm{s}} \approx 5\,n_{\mathrm{cr}}$, where $n_{\mathrm{cr}} \approx 1.75 \times 10^{21}\ \mathrm{cm}^{-3}$ is the critical electron density for the free-space laser wavelength $\lambda_{\mathrm{fs}} = 0.8\,\mu\mathrm{m}$. The saturation density n_{s} is the maximum density that can be reached when every molecule is ionized. The laser pulse length was assumed to be equal to 70 fs in our simulations. At the entrance of the simulation domain the pulse was represented by a Gaussian beam that would focus into a spot of radius $r_{\mathrm{spot}} = 2\,\mu\mathrm{m}$ in free space.

The FDTD code solves equations (1)–(3) numerically and thus simulates linear and nonlinear laser propagation in the medium, plasma generation, ionizational and collisional energy losses as well as laser interaction with the plasma free particles. The accuracy of the simulations is limited by the uncertainties in some of the parameters involved. The third-order susceptibility, $\chi^{(3)}$, of pure PMMA is relatively well known and is estimated to be

3×10^{-14} esu [58]. However, σ_3 in PMMA is not well known. We assume that it is comparable to other materials with three-photon resonance and therefore replaces the value of σ_3 in PMMA with that of borosilicate glass (the bandgap of borosilicate glass is ~4 eV, while that of PMMA is ~3.7 eV), $\sigma_3 \approx 7 \times 10^{17}$ cm^3 ps^{-1} (cm^2 TW^{-1})^3 [40]. However, it is important to note that an order of magnitude change in σ_3 does not significantly affect the results.

Another source of uncertainty is the damping factor Γ in equation (2). This factor, which represents the laser energy deposition in the collisional plasma caused by the inverse bremmstrahlung heating, is of the order of collision frequency ν_e of the plasma electrons and can be estimated using the Spitzer formula [56]

$$\nu_e\,[\mathrm{s}^{-1}] = 2.9 \times 10^{-6} n\,[\mathrm{cm}^{-3}] \lambda\,[\mathrm{cm}]\, T_e^{-3/2}\,[\mathrm{eV}]. \tag{4}$$

Since the interaction process is non-equilibrium, the electron temperature T_e can be estimated to only an order of magnitude. The electrons excited into the conduction band after absorbing three photons (~4.6 eV) will have a kinetic energy of the order of ~1 eV. This energy is much larger than the Fermi energy, estimated to be ~0.15 eV for a plasma with $n = n_{cr}$. Therefore, one can use a classical approach to estimate the temperature, which thus will be of the order of the quiver energy of the free electron in the oscillating laser field (~10 eV at an intensity of ~10^{14} W cm^{-2}). $n = n_{cr}$ is used to evaluate equation (4), resulting in the collision frequency $\nu_e \approx 0.1$ fs^{-1}, which is used in our simulations. A similar value for collision frequency can be obtained using models for strongly coupled plasmas [59]. The rationale for choosing $n = n_{cr}$ is as follows. When the plasma density is overcritical the laser is reflected back without depositing much energy in the plasma, irrespective of the collision frequency. For undercritical plasma the modification patterns were found to be insensitive to Γ [19]. Therefore it is anticipated that the interaction physics is most sensitive to the particular value of electron collision frequency when the plasma density is near-critical or slightly overcritical.

The electron temperature T_e can also be estimated using a quantum mechanical approach, instead of classical. A similar value of $T_e = 12$ eV was obtained for dielectric breakdown in fused silica [60]. The choice of T_e was found in our calculations to not have any substantial influence on the shape of the ablation spot in the range of 3–30 eV. However, if T_e is too small (<1 eV) the asymmetry in the spot disappears, whereas for higher temperatures the asymmetry becomes more prominent.

The accuracy of the simulation is also limited by the fact that we use a fixed value for $\chi^{(1)}$ of the sample while in reality it varies during the entire interaction process. The refractive index of the sample is time dependent due to depletion of bound electrons and can decrease as more electrons are removed into the conduction band by the ultrashort laser pulse. It is therefore reasonable to choose a linear index of refraction that is slightly smaller ($n_0 = 1.3$) than the actual unperturbed value of ~1.5. However, the refractive index modification due to the presence of free electrons is fully taken into account by the plasma current $\vec{J}_P$ that contributes to $\vec{J}$ in equation (1).

We also assume that the energy transfer from electrons to the lattice, which occurs on a much longer time scale compared to the duration of the laser pulse, is localized and coincides with the shape of the plasma. This is justified by the fact that (i) recent calculations [57] demonstrate that there is no difference between damage criteria when either the free electron density or the internal lattice energy is considered. (ii) Even energetic electrons (10 eV) travel a distance of only a fraction of the spot size within the recombination time or even longer.

For this reason, an asymmetry in the plasma profile, if any, will translate into an asymmetry in the ablated spot.

In addition, there are other approximations made in the model given by equations (1)–(3). Firstly, we neglect the higher-order nonlinearities that can be important for intense laser interactions. Secondly, we consider susceptibilities $\chi^{(1)}$ and $\chi^{(3)}$ and the ionization cross-section σ_3 to be frequency independent. We also neglect processes such as avalanche ionization. Furthermore, we assume that the damping factor Γ in equation (2) is a constant, whereas it actually depends on the plasma density and temperature, which in turn depends on the overall interaction dynamics. Therefore, the results presented below are expected to only provide qualitative agreement with the experiments.

3.2. Characterization of the ablation crater

We now demonstrate that polarization-dependent ablation of PMMA arises due to the interaction of the laser pulse with the plasma produced by the leading edge of the pulse. Such a light–plasma interaction leads to local field enhancements either parallel or perpendicular to the laser polarization, depending on the plasma density.

Figure 6(a) shows the maximum plasma particle density in units of critical density as a function of the position of the laser focus in the PMMA sample. The plasma density is maximum and is overcritical on the surface and decreases rapidly to below the critical value as the laser focus is moved inside the sample by more than a Rayleigh length ($\sim$16 μm for a focal spot radius of 2 μm used in the calculation). When the laser is focused deep inside the bulk PMMA, the incident pulse undergoes defocusing by the plasma generated by the leading edge of the pulse [19]. As a result, the intensity of the laser pulse at the focus is clamped which results in the generation of undercritical plasma [19, 61]. As the laser focus is shifted closer to the surface, the volume of the undercritical plasma generated by the pulse leading edge is decreased, thus decreasing the plasma negative lens effect.

A typical plasma particle density profile of the laser-generated plasma in the polarization plane is shown in figure 6(b). When the laser is focused right at the sample surface, there is a very thin shell of overcritical plasma that is surrounded by undercritical plasma of a relatively large volume with a diverging shape. This diverging shape is the result of a laser defocusing by the negative plasma lens that surrounds the overcritical disc. The undercritical plasma right behind the disc is created by the leading edge of the laser pulse. When the plasma is undercritical ($n \sim 0.5n_{cr}$), it leads to refractive index modification [62]. So the actual plasma density value that is required for the ablation must lie somewhere in the critical range.

The plasma particle density profile at the sample surface perpendicular to the direction of laser propagation is shown in figure 6(c). One can clearly see elongation of the overcritical plasma along the polarization direction in the central region of the laser focus. The overcritical plasma electrons oscillate in phase with the laser field, leading to field enhancement at the edges of the plasma in the direction of laser polarization, akin to metal nanoparticles. Faster plasma growth in regions with enhanced fields results in elongation along the polarization direction. In the undercritical plasma regions, elongation is, in contrast, in the direction perpendicular to laser polarization. Electrons in the undercritical plasma oscillate out of phase with the laser, resulting in suppression of the field at the plasma edge in the direction of polarization. In this case, the fields are enhanced all along the plane perpendicular to the laser polarization. Signatures

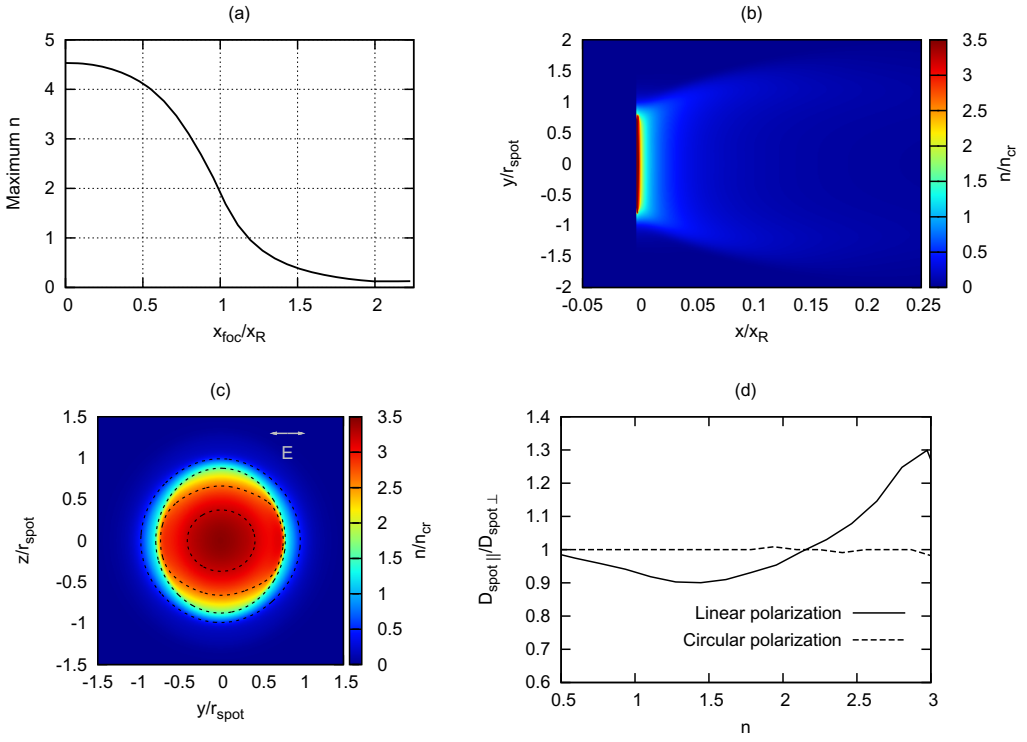

Figure 6. Results of numerical simulations for an incident pulse of intensity 10^{14} W cm^{-2} interacting with a PMMA sample. (a) Maximum plasma electron particle density on the laser axis (in units of critical density) as a function of geometrical position of the laser focus in units of the Rayleigh length ($\sim$16 μm). (b) Plasma density profile in the polarization plane passing through the laser axis. The surface is located at $x = 0$. The abscissa is in units of Rayleigh length and the ordinate is in units of spot radius. (c) Plasma density profile at the surface of the sample. The distances are in units of spot radius. (d) Quantitative characterization of the spot elongation along the polarization versus plasma density in units of critical density for linear (solid line) and circular (dashed line) laser polarizations.

of such polarization dependence have been observed in the laser interaction inside bulk fused silica where the plasma is undercritical [17–19].

The plasma edge (transition from overcritical to undercritical plasma) is smooth since the transverse shape of the ablation spot is approximately Gaussian (with a size $\sim\sqrt{3}$ times smaller than the laser beam size, for the three-photon ionization process). For this reason, the ablation process is characterized by the two competing effects: (i) field suppression in the polarization direction at locations where the plasma is undercritical, i.e. at distances far from the centre of the laser focus (figure 6(c)); and (ii) field enhancement in the polarization direction at positions where the plasma is overcritical, i.e. close to the centre of the laser focus. The exact shape of the ablation crater is determined by these competing effects, as well as the minimum plasma density that is required for the onset of the actual ablation process.

Quantitative characterization of the elongation of the ablation spot can be made by determining the boundary of the spot for a specified plasma density. Figure 6(d) shows the

ratio of the ablation spot along two orthogonal directions as a function of the plasma density for linear (solid line) and circular polarizations (dashed line). A ratio of unity corresponds to a circular ablation spot with no elongation. For linearly polarized light, the elongation is parallel (perpendicular) to the laser polarization when plasma density $n \gtrsim 2\,n_{\rm cr}$ (or otherwise). Since in a collision-dominated plasma, reflectivity approaches unity only when its density is well above the critical density, this value seems reasonable. When plasma density is very low ($n \lesssim 0.5 n_{\rm cr}$), field enhancement is negligible and one does not expect any elongation.

Comparing figure 6(d) with figure 3, one can conclude that the plasma density corresponding to the ablation threshold is of the order of $n \sim 2\,n_{\rm cr}$. The dependence of elongation on plasma density is then in agreement with experimental observations (figure 3): (i) no elongation close to threshold pulse energies and (ii) larger asymmetry of the ablation craters for higher pulse energies (corresponding to a plasma density well above the critical density). Moreover, there is no elongation of the ablation spot for circularly polarized light irrespective of the plasma density, as observed in the experiments. Given the approximate nature of our model, a maximum of $\sim$30% elongation for linearly polarized light is in good agreement with the experimental value of $\sim$40%.

The simulations also indicate that the energy deposited in the region with an undercritical plasma (figure 6(b)) is of the order of ten to a few tens of per cent of pulse energy. The energy deposition mechanisms include multiphoton absorption and collisional energy absorption inside the plasma. As the plasma recombines (which happens on the ps time scale compared to the ns time scale of hydrodynamic processes [63]), this energy is converted into heat. Considering that the heat capacity of PMMA is in the range of $\sim 1\,{\rm J\,(g\,K)^{-1}}$ [64], an order-of-magnitude estimation shows that deposition of $\sim 1\,\mu$J of laser energy in $\sim 10^3\,\mu{\rm m}^3$ (estimated from figure 6(b)) is sufficient to heat up the PMMA inside this volume by $\sim 10^3$ K, i.e. above its boiling point ($\sim$200 °C). We conclude that it is this localized boiling that has resulted in the porous structures observed in the experiment.

Another possible mechanism that can give rise to porosity could be multiple filamentation of the incident pulse while propagating through the medium that leads to severe localization of the pulse energy. Although our simulations rule out this possibility for pure PMMA, we found that this mechanism can occur in highly nonlinear media. For example, the third-order susceptibility $\chi^{(3)}$ in PMMA can be enhanced significantly by doping [58]. When a high value of $\chi^{(3)}$ ($= 3 \times 10^{-12}$ esu) is used in the simulation sub-surface, multiple filamentation is observed for laser intensities above the ablation threshold, as shown in figure 7, where the plasma density profiles (in units of $n_{\rm cr}$) at time moments well after the laser passage are plotted.

Figure 7(b) shows the plasma density inside doped PMMA in the plane perpendicular to the laser polarization for the peak laser intensity $I = 10^{13}\,{\rm W\,cm^{-2}}$. Upon entering the medium, the pulse is immediately self-focused. Due to the very large nonlinearity, the self-focused pulse eventually experiences filamentation. The laser intensity inside the individual filaments reaches considerably high values leading to the material ionization along the filaments. However, the maximum surface plasma density in this simulation is $n_{\rm max} \approx 0.07 n_{\rm cr}$, which is not expected to appreciably damage the surface of the material [62]. At later time scales, hydrodynamic expansion of the hot material under the surface will lead to swelling of the surface similarly to that observed in figures 2(a) and (b).

As the incident laser intensity is increased, the plasma density at the surface grows and reaches values of several $n_{\rm cr}$ for intensities $I \sim 10^{14}\,{\rm W\,cm^{-2}}$. For this high plasma density, the material ablates directly from the surface. However, the leading part of the laser pulse that

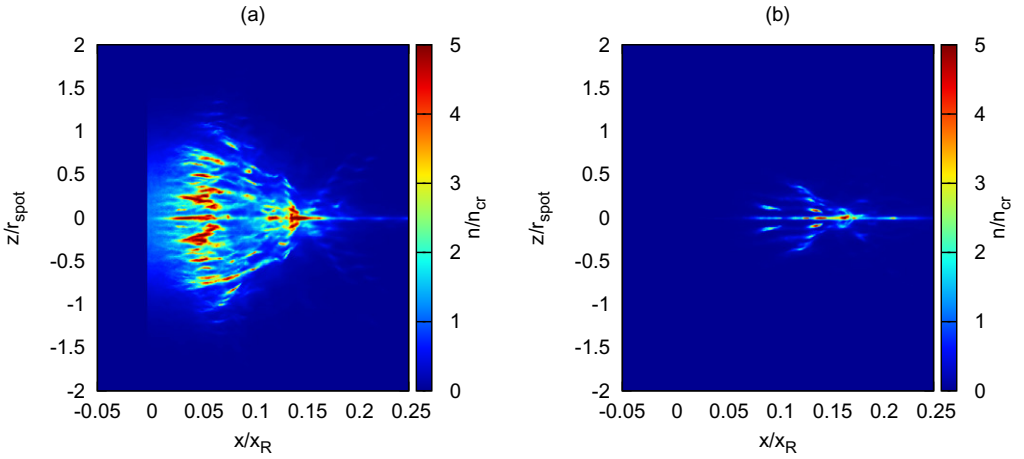

Figure 7. Simulation of the ablation process in doped PMMA. Plasma density generated inside the material when the laser pulse that is focused on the surface of PMMA located at origin propagates in the $+\hat{x}$-direction and is polarized along the $\hat{y}$-direction. The abscissa is in units of Rayleigh length, while the ordinate is in units of spot radius. (a) The laser intensity is above the ablation threshold ($10^{14}\,\mathrm{W\,cm^{-2}}$); (b) the laser intensity is below the ablation threshold ($10^{13}\,\mathrm{W\,cm^{-2}}$). The material surface is located at $x = 0$. The plasma density is measured in units of n_{cr}.

has not been reflected by the surface plasma propagates inside the material and experiences filamentation in the same way as described above. This produces a rich internal structure of the under-surface plasma (figure 7(a)) that can lead to induced porosity. The intensity within the filaments can be high enough that the plasma density can be overcritical. This severe localization of laser energy within the focal volume leads to nano-explosions ejecting out of the material. At the same time, material is removed from the surface, resulting in the material becoming porous. Whereas explosive boiling is the origin of porosity in pure PMMA, in doped PMMA a sub-surface localization of pulse energy in the form of multiple filaments could also give rise to porosity, in addition to the causative factor of hydrodynamic expansion that leads to explosive boiling. Since filamentation is a propagation effect, the pores would originate deep inside the sample as compared to the hydrodynamics process that is restricted to the sub-surface. Analyzing the ablated region along the propagation direction may allow one to distinguish the two mechanisms.

4. Conclusions

In this paper, we show that femtosecond laser ablation of PMMA is polarization dependent in the form of elongated craters (for a stationary focus) and quasi-periodic structures (for line ablation) parallel to laser polarization. Simulations show that elongation of ablation craters can be attributed to a field enhancement during the interaction of an intense light pulse with the overcritical transient plasma produced by the pulse's leading edge. The present work on polarization-dependent ablation (single pulse regime) combined with our previous work on laser-induced periodic structures in fused silica [17] (in the multiple pulse regime) provides

insights into the crucial role played by transient plasmas in the interaction of intense ultrashort light pulses with dielectric materials. Light–plasma interaction influences the energy coupling to the solid by redistributing the local fields in the focal region with respect to the direction of polarization of the incident laser field. Local field enhancement is determined by the plasma density and its signatures are embedded in the interaction region. This effect is not unique to a specific material and would occur whenever there is sufficient nonlinearity in the intensity dependence of the ionization process in order for the field enhancements to produce a noticeable effect in the dielectric. We therefore expect that light–plasma effects will play a less significant role for longer pulse durations, where collisional ionization becomes the dominant process [21]. Polarization-dependent ablation will have an impact on micro-machining, and its effects can be minimized by using either pulse energies close to ablation threshold or circularly polarized light.

Acknowledgments

The authors acknowledge Robert Boyd, Paul Corkum and Thomas Brabec for fruitful discussions and the Natural Science and Engineering Research Council, Canadian Foundation for Innovation and the Ontario Ministry of Economic Development and Innovation for financial support.

References

[1] Seideman T 1995 *J. Chem. Phys.* **103** 7887
Staplefeldt H and Seideman T 2003 *Rev. Mod. Phys.* **75** 543
[2] Friedrich B and Herschbach D 1995 *Phys. Rev. Lett.* **74** 4623
[3] Larsen J J *et al* 2000 *Phys. Rev. Lett.* **85** 2470
Bisgaard C Z *et al* 2004 *Phys. Rev. Lett.* **92** 173004
[4] Niikura H *et al* 2002 *Nature* **417** 917–22
[5] Baker S *et al* 2006 *Science* **312** 424–7
[6] Corkum P B and Krausz F 2007 *Nature Phys.* **3** 381
[7] Krüger M, Schenk M and Hommelhoff P 2011 *Nature* **475** 78
[8] Davis K M *et al* 1996 *Opt. Lett.* **21** 1729
[9] Chan J W, Huser T, Risbud S and Krol D M 2001 *Opt. Lett.* **26** 1726
[10] Gertsvolf M *et al* 2008 *Phys. Rev. Lett.* **101** 243001
[11] Litvinyuk I V *et al* 2003 *Phys. Rev. Lett.* **90** 233003
[12] Pavicic D *et al* 2007 *Phys. Rev. Lett.* **98** 243001
[13] Pearlman J S, Thomson J J and Max C E 1977 *Phys. Rev. Lett.* **38** 1397
[14] Dinger R, Rohr K and Weber H 1987 *Laser Part. Beams* **5** 691
[15] Tanabe K 2008 *J. Phys. Chem.* C **112** 15721
[16] Shimotsuma Y *et al* 2003 *Phys. Rev. Lett.* **91** 247405
[17] Bhardwaj V R, Simova E, Rajeev P P, Hnatovsky C, Taylor R S, Rayner D M and Corkum P B 2006 *Phys. Rev. Lett.* **96** 057404
[18] Rajeev P P *et al* 2007 *J. Phys. B: At. Mol. Opt. Phys.* **40** S273
[19] Popov K I, McElcheran C, Briggs K, Mack S and Ramunno L 2011 *Opt. Express* **19** 271
[20] Taylor R S *et al* 2007 *Opt. Lett.* **32** 2888
[21] Hnatovsky C *et al* 2005 *Appl. Phys. Lett.* **87** 014104
[22] Hnatovsky C *et al* 2006 *Appl. Phys.* A **84** 47
[23] Taylor R S, Simova E and Hnatovsky C 2008 *Opt. Lett.* **33** 1312

[24] Hnatovsky C, Shvedov V, Krolikowski W and Rode A 2011 *Phys. Rev. Lett.* **106** 123901
[25] Birnbaum M 1965 *J. Appl. Phys.* **36** 3688
[26] Young J F, Sipe J E and van Driel H M 1984 *Phys. Rev.* B **30** 2001
Young J F, Sipe J E and van Driel H M 1983 *Opt. Lett.* **8** 431
[27] Guosheng Z, Fauchet P M and Siegman A E 1982 *Phys. Rev.* B **26** 5366
[28] Preston J S, Van Driel H M and Sipe J E 1989 *Phys. Rev.* B **40** 3942
[29] Varel H, Wahmer M, Rosenfeld A, Ashkenasi D and Campbell E E B 1998 *Appl. Surf. Sci.* **127–129** 128
[30] Ozkan A M, Malshe A P, Railkar T A, Brown W D, Shirk M D and Molian P A 1999 *Appl. Phys. Lett.* **75** 3716
[31] Yasumaru N, Miyazaki K and Kiuchi J 2002 *Appl. Phys.* A **76** 983
[32] Bonse J, Baudach S, Krüger J, Kautek W and Lenzner M 2002 *Appl. Phys.* A **74** 19
[33] Borowiec A and Haugen H K 2003 *Appl. Phys. Lett.* **82** 4462
[34] Bolle M and Lazare S 1993 *Appl. Surf. Sci.* **65/66** 349
[35] Young J, Preston J, van Driel H and Sipe J 1983 *Phys. Rev.* B **27** 1155
[36] Huang M, Zhao F L, Cheng Y, Xu N S and Xu Z Z 2009 *ACS Nano* **3** 4062
[37] Han Y, Zhao X and Qu S 2011 *Opt. Express* **19** 19150
[38] Baudach S, Bonse J and Kautek W 1999 *Appl. Phys.* A **69** S395
[39] Venkatakrishnan K, Tan B, Stanley P and Sivakumar N R 2002 *J. Appl. Phys.* **92** 1604
[40] Kruger J and Kautek W 2004 *Adv. Polym. Sci.* **168** 247
[41] Miotello A and Kelly R 1995 *Appl. Phys. Lett.* **67** 3535
Miotello A and Kelly R 1999 *Phys. Rev.* E **60** 2616
[42] Zhigilei L V *et al* 2003 *Chem. Rev.* **103** 321
[43] Craciun V *et al* 2002 *Appl. Surf. Sci.* **186** 288
[44] Haglund R F Jr and Ermer D R 2000 *Appl. Surf. Sci.* **168** 258
[45] Perez D and Lewis L J 2002 *Phys. Rev. Lett.* **89** 255504
Perez D and Lewis L J 2003 *Phys. Rev.* B **67** 184102
[46] Lorazo P, Lewis L J and Meunier M 2003 *Phys. Rev. Lett.* **91** 225502
[47] Sokolowski-Tinten K *et al* 1998 *Phys. Rev. Lett.* **81** 224
[48] Anisimov S I *et al* 1999 *Appl. Phys.* A **69** 617
[49] Zhakhovski V V, Nishihara K, Anisimov S I and Inogamov N A 2000 *JETP Lett.* **71** 167
[50] Agranat M B *et al* 2007 *Appl. Surf. Sci.* **253** 6276
[51] Savolainen J-M, Christensen M S and Balling P 2011 *Phys. Rev.* B **84** 193410
[52] Baudach S, Bonse J, Kruger J and Kautek W 2000 *Appl. Surf. Sci* **154–155** 555
[53] Rajeev P P *et al* 2006 *Phys. Rev. Lett.* **97** 253001
[54] Mulser P, Cornolti F and Bauer D 1998 *Phys. Plasmas* **5** 4466
[55] Peñano J R, Sprangle P, Hafizi B, Manheimer W and Zigler A 2005 *Phys. Rev.* E **72** 036412
[56] Huba J D 2004 NRL Plasma Formulary (Naval Research Laboratory) p 34
[57] Rethfeld B *et al* 2010 *Appl. Phys.* A **101** 19
[58] D'Amore F, Lanata M, Pietralunga S M, Gallazzi M C and Zerbi G 2004 *Opt. Mater.* **24** 661–5
[59] Cauble R and Rozmus W 1985 *Phys. Fluids* **28** 3387
[60] Kaiser A, Rethfeld B, Vicanek M and Simon G 2000 *Phys. Rev.* B **61** 11437
[61] Rayner D M, Naumov A and Corkum P 2005 *Opt. Express* **13** 3208
[62] Sudrie L *et al* 2002 *Phys. Rev. Lett.* **89** 186601
[63] Mézel C, Hallo L, Bourgeade A, Hébert D, Tikhonchuk V T, Chimier B, Nkonga B, Schurtz G and Travaillé G 2008 *Phys. Plasmas* **15** 093504
[64] Soldera A, Metatla N, Beaudoin A, Said S and Grohens Y 2010 *Polymer* **51** 2106–11